

Article

The Effects of Altering the Center of Pressure in Standing Subjects Exposed to Foot-Transmitted Vibration on an Optimized Lumped-Parameter Model of the Foot

Stefano Marelli ^{1,*} , Delphine Chadeaux ^{1,2,3}, Katie Goggins ⁴, Tammy Eger ⁴ , Diego Scaccabarozzi ¹  and Marco Tarabini ¹ 

- ¹ Mechanical Department, Politecnico di Milano, 20156 Milano, Italy; delphine.chadeaux@sorbonne-paris-nord.fr (D.C.); diego.scaccabarozzi@polimi.it (D.S.); marco.tarabini@polimi.it (M.T.)
 - ² Institut de Biomécanique Humaine Georges Charpak, IBHGC, Université Sorbonne Paris Nord, UR 4494, F-93000 Bobigny, France
 - ³ Département STAPS, Université Sorbonne Paris Nord, F-93000 Bobigny, France
 - ⁴ Centre for Research in Occupational Safety and Health, Laurentian University, Sudbury, ON P3E 2C6, Canada; kx_goggins@laurentian.ca (K.G.); tege@laurentian.ca (T.E.)
- * Correspondence: stefano1.marelli@polimi.it



Citation: Marelli, S.; Chadeaux, D.; Goggins, K.; Eger, T.; Scaccabarozzi, D.; Tarabini, M. The Effects of Altering the Center of Pressure in Standing Subjects Exposed to Foot-Transmitted Vibration on an Optimized Lumped-Parameter Model of the Foot. *Vibration* **2021**, *4*, 893–905. <https://doi.org/10.3390/vibration4040050>

Academic Editors: Setsuo Maeda, Ying Ye, Cyriel Diels and Jelte Bos

Received: 5 August 2021

Accepted: 26 November 2021

Published: 30 November 2021

Publisher's Note: MDPI stays neutral with regard to jurisdictional claims in published maps and institutional affiliations.



Copyright: © 2021 by the authors. Licensee MDPI, Basel, Switzerland. This article is an open access article distributed under the terms and conditions of the Creative Commons Attribution (CC BY) license (<https://creativecommons.org/licenses/by/4.0/>).

Abstract: Many workers are exposed to foot-transmitted vibration, which can lead to the development of vibration-induced white foot: a debilitating condition with neurological, vascular and osteoarticular symptoms. To design effective prevention mechanisms (i.e., boots and insoles) for isolating workers from vibration exposure, continued model development of the foot's biodynamic response in different positions is necessary. This study uses a previously developed model of the foot–ankle system (FAS) to investigate how altering the center of pressure (COP) location can change the biodynamic response of the FAS to standing vibration exposure. Formerly published experimental responses for apparent mass and transmissibility at five anatomical locations in three COP positions were used to optimize the model. Differences occurred with the Kelvin–Voigt elements used to represent the soft tissues of the foot sole: at the heel, the distal head of the metatarsals and distal phalanges. The stiffness increased wherever the COP was concentrated (i.e., forward over the toes or backward over the heel). The variability of the model parameters was always greatest when the COP was concentrated in the heel. This suggests future FAS models need to more clearly address how the soft tissue of the plantar fat pad is modelled.

Keywords: whole-body vibration; biomechanical response; posture; standing vibration

1. Introduction

The foot–ankle system (FAS) is the primary exposure point for foot-transmitted vibrations (FTV). Exposure to FTV for prolonged periods can increase the risk of the vibration-induced white foot (VIWft) [1–3]. The effects of VIWft can include neurological, vascular and osteoarticular symptoms. Neurological symptoms include numbness and tingling in the toes or a reduced sense of touch and temperature. Vascular symptoms can include increasing loss of circulation which could lead to toe blanching and necrosis. Osteoarticular symptoms can include bone or joint damage and muscular fatigue [4,5]. In order to prevent injury sustained from FTV exposure, effective personal protective equipment (PPE), such as boots and insoles [6] must be designed to address the biodynamic response (i.e., transmissibility) or the degree to which vibration is transmitted through the foot. However, few studies have explored the impact of FTV exposure as the forces on different portions of the foot varies (i.e., apparent mass and changes in the center of pressure (COP)) [7].

Models are used to simulate the biodynamic responses of the anatomy of interest [8], in this case, the FAS [9,10], to limit human exposure to vibration while testing possible

solutions. Simplified lumped-parameter (i.e., Kelvin–Voigt) models of standing subjects have been developed to reproduce the apparent mass measured at the contact surface (i.e., the floor) [7,8]. However, these models are not suitable to reproduce the FAS biodynamic response as they do not include a separate foot component. A biomechanical model made of two rigid bodies connected by a hinge and a horizontal tension stiffness has been used to evaluate the energy storage of the plantar fascia [11] and to investigate the role of the inclination of the calcaneus. An improved and asymmetric version of this model investigated the role of the plantar fascia in the load-bearing aspect of the foot [9]. This hinge model was then used as the foundation for developing three lumped-parameter models that more specifically simulate the effects of FTV on the FAS [10,12,13].

The structure of the first FTV lumped-parameter model included masses for the tibia, calcaneus and talus, navicular, three cuneiforms and three metatarsals [10]. Unfortunately, this model was validated using transmissibility data from measurements at the medial malleolus and tibial tuberosity of seated subjects, with variations in the load on the knees within a frequency range of 10–50 Hz at 5 Hz increments [14]. Therefore, this model provides a poor estimation of the transmissibility effects of FTV exposure for the FAS. Using a similar structure, with an additional upper body mass to simulate the whole-body resonant frequency more effectively, a two-dimensional model of the FAS [12] was optimized. This optimized model uses the transmissibility response of the foot at five anatomical locations of 21 participants [15] and the apparent normalized mass of 10 male participants [16]. This model demonstrated good similarity with the measured biodynamic responses of the foot but was limited to a barefoot natural standing position.

Reference functions for model calibration can include vibration transmissibility, driving-point response (i.e., apparent mass), or a combination of the two [8]. Transmissibility measurements from 24 anatomical locations on the foot indicated changes in the center of pressure (COP) (i.e., towards the forefoot and rearfoot) altered the transmissibility response at the different locations [17]. Changes to the COP, the calcaneal angle [11] and the height of the calcaneus [18] have also been shown to lead to variations in the respective models. In a previous experiment where the apparent mass and transmissibility of subjects exposed to whole-body vibration in different postures were measured, the apparent mass at the driving point was found to change due to different knee angles [19]. However, other experiments have shown that the apparent mass at the driving point did not change significantly in the case of a forward leaning straight leg posture [16]. Therefore, the effects of varying the COP need to be considered in order to establish an effective FAS model for testing possible PPE materials.

The model structure was reduced to a four degrees-of-freedom (DOF) lumped-parameter model of the FAS and was tested using transmissibility measurements while participants were in three COP positions (natural, forward towards the toes and backward towards the rearfoot) [13]. Although the model performed well when the COP was natural or forward towards the toes, the optimization was inadequate when the COP was in the heel.

Thus, the purpose of this study was to continue to build on the four-segment lumped-parameter model that was developed, as it includes a segment for the toes and an expanded frequency range (10 to 100 Hz) [12]. This model was selected as it performed well using natural standing position transmissibility and apparent mass data but has yet to be optimized when altering the COP. The study's central hypothesis is that variation in the COP will change the equivalent stiffness and damping values of the FAS, with this model more effectively simulating the transmissibility response when the COP is towards the heel [13]. It is anticipated that the stiffness parameters at the heel will increase when the COP is in the rearfoot and similarly for the toes when the COP is in the forefoot. Once an effective model of the FAS has been established for multiple COP positions, it can be used to reproduce the interaction mechanism between the human body and vibrating surface (i.e., different types of industrial equipment) [20]. In addition, the model could give new insights into assessing health risk for workers exposed to FTV, taking into account the effect of posture. Further,

the model can be used to estimate the vibration reduction of devices (i.e., PPE) [21], as is the natural progression of hand-transmitted vibration modelling [22].

2. Materials and Methods

This study incorporated a formerly developed lumped-parameter model of the FAS [12] and two previously collected experimental data sets as the reference functions for optimization [15–17]. Transmissibility is the ratio between the input vibration from the platform to the FAS and the vibration of the FAS at a given anatomical location [7]. Three sets of transmissibility responses from the foot at five anatomical locations were used, incorporating a variation in COP. The COP was in a natural (i.e., centered) position [15], pushed forward towards the toes and backwards towards the heel [17] (Figure 1a). The apparent mass is the transfer function between the input acceleration and the exchanged force [7]. As the apparent mass at the driving point has not been found to differ significantly with forward leaning straight leg postures, an experimental data set incorporating the apparent mass of ten participants was used [16]. The FAS model incorporates four-foot segments and was chosen to correctly represent foot transmissibility at five different locations (rearfoot, ankle, midfoot, forefoot and toes) (Figure 1b) [12,23], as it has previously demonstrated acceptable error for transmissibility data in the natural standing position. The upper part of the body is modelled with a simple two-masses model to reconstruct the apparent mass [24].

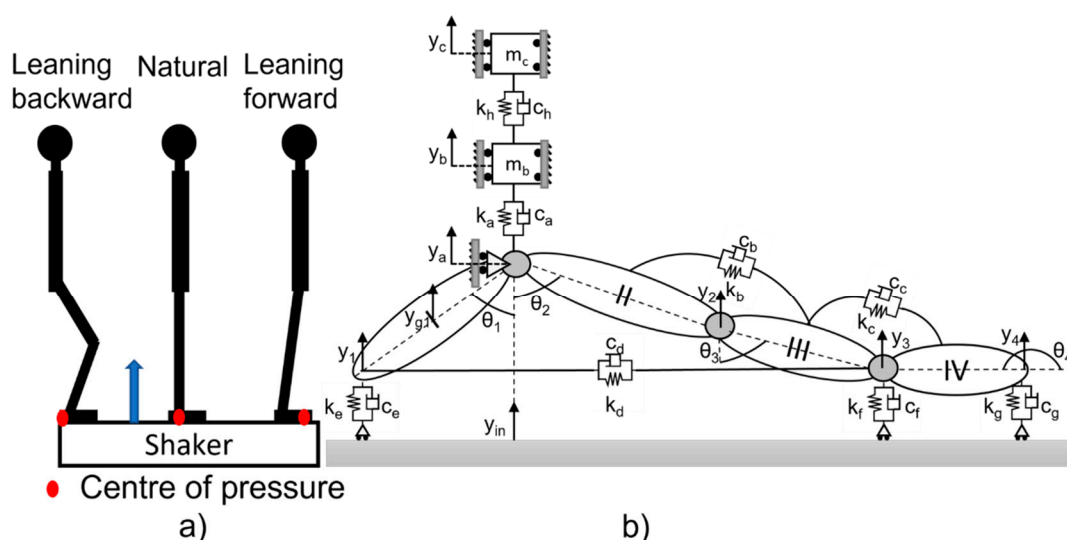


Figure 1. (a) Different body positions and the effect on the center of pressure [17]; (b) Six degrees-of-freedom model of the foot–ankle system composed of six rigid elements connected by Kelvin–Voigt models of stiffness (k_i) and damping (c_i) [12].

2.1. Experimental Datasets

The experimental transmissibility (T_f^i) and apparent mass (AM_f) data were collected during three previous studies [15–17]. Twenty-one subjects were exposed to vertical vibration from the 10–100 Hz frequency range. Foot transmissibility was acquired at rearfoot, ankle, midfoot, forefoot and toes (Figure 2a) while subjects assumed natural [15], forward leaning and backward leaning standing positions on the platform [17]. The COP was measured using Pedar-Expert insoles (Version 11.3.12, Munich, Germany) while the subjects were off the vibration platform, and a plumbline was attached to the right hip with a marker on the right foot for each COP position [17]. While on the vibration platform, the subject would assume the COP position using the plumbline guide before the vibration exposure for each anatomical location.

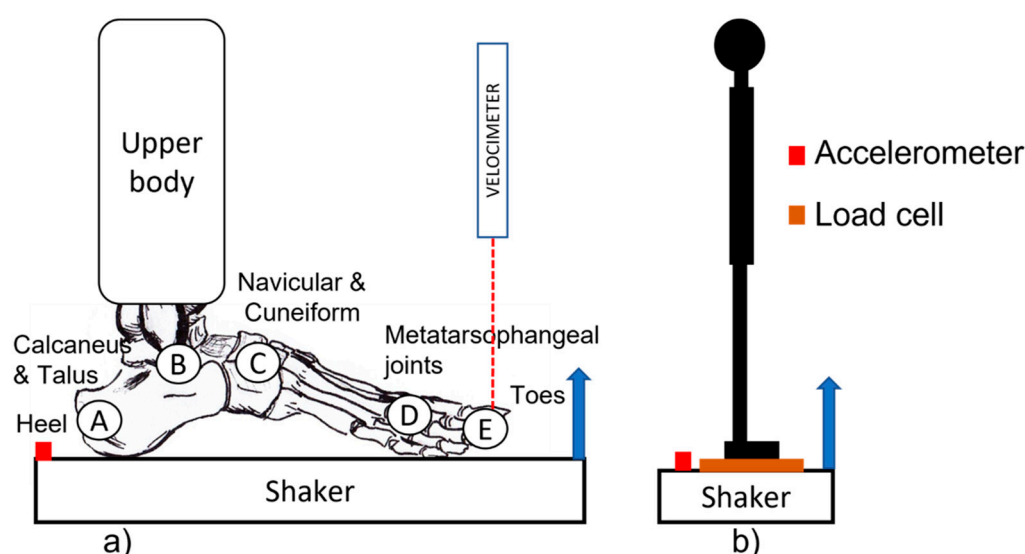


Figure 2. (a) Schematic representation of the experimental setup used to measure foot transmissibility. An accelerometer measured the vertical acceleration at the vibrating plate while a velocimeter measured the output velocity at 24 locations that can be grouped into zones from A to E [15,17]. (b) Schematic representation of the experimental setup used to measure apparent mass. A load cell measured the force at the driving point while an accelerometer measured the vertical acceleration [16].

The apparent mass mean curve was collected while ten subjects stood in their natural posture and were exposed to vertical vibration within the 2–20 Hz frequency range (Figure 2b) [16]. Since changing COP has been found to have minimal effects on the apparent mass curve [16], apparent mass for backward and forward leaning COP positions have been assumed to be equal to the natural COP apparent mass curve.

2.2. Foot Model Description

The FAS model is composed of six rigid elements (Figure 1b) [12]: two masses were used to represent the upper body ($m_b = 20.09$ kg and $m_c = 13.79$ kg) [24] and four segments (I to IV), with their inertial and geometric properties reported in Table 1. The segments are connected through Kelvin–Voigt models to reproduce the viscoelastic properties of tissues and ligaments with stiffness parameters (k_{a-h}) and damping (c_{a-h}). The linear DOF of the system is the vertical displacements of the ankle (y_A), and of the upper body masses (y_B and y_C). The rotational DOF includes rotation of the rearfoot (θ_1), midfoot (θ_2), forefoot (θ_3) and toes (θ_4). The constrained DOF is the vertical displacement of the vibrating surface (y_{in}), which applies the harmonic displacement to the sole of the foot. The transmissibility response of the foot is evaluated in the middle of the rearfoot (y_1), the junction between midfoot and forefoot (y_2), the junction between forefoot and toes (y_3) and at the distal end of the toes (y_4). The linearized equations of motion have previously been described (Appendix B of [12]).

Table 1. Inertial and geometrical properties of foot segments [25–27].

Segment	Inertia [kg m ²]	Length [m]	Mass [kg]
Rearfoot I	28×10^{-5}	0.046	0.294
Midfoot II	10×10^{-7}	0.085	0.294
Forefoot III	14×10^{-6}	0.070	0.196
Toes IV	15×10^{-7}	0.060	0.098

The expression of the transmissibility from the vibrating ground ($r_{in} = y_{in}$) to five-foot locations has been computed considering the linearized equations of the FAS model [28]. The response of the seven DOF (r_{dof}) can be written as Equation (1):

$$\left[\tilde{T}\right] = \frac{r_{dof}}{r_{in}} = \frac{-(-\Omega^2[M_{FC}] + i\Omega[C_{FC}] + [K_{FC}])}{(-\Omega^2[M_{FF}] + i\Omega[C_{FF}] + [K_{FF}])}, \quad (1)$$

where I is the imaginary unit, Ω is the angular frequency, and $M_{FF,FC}$, $C_{FF,FC}$ and $K_{FF,FC}$ are the free-free (FF) and free-constrained (FC) components of the global mass (M), damping (C) and stiffness (K) matrices, respectively. Matrices $M_{FF,FC}$, $R_{FF,FC}$ and $K_{FF,FC}$ were composed of the geometrical and inertial characteristics provided in Table 1, and the stiffness ($k_{a...h}$) and damping ($c_{a...h}$) parameters. The transmissibility curves (\tilde{T}^1 , \tilde{T}^2 , \tilde{T}^3 , \tilde{T}^4 and \tilde{T}^5) between the selected vertical velocities (\dot{y}_{g1} , \dot{y}_2 , \dot{y}_3 , \dot{y}_4 and \dot{y}_A) and the vibrating ground velocity (\dot{y}_{in}) were obtained considering the geometrical relationship with the free DOF of the linearized equation of motion of the system [12].

The normalized apparent mass of the model was computed according to Equation (2):

$$\widetilde{AM} = \frac{(y_1 - y_{in})k_e + (\dot{y}_1 - \dot{y}_{in})c_e + (y_3 - y_{in})k_f + (\dot{y}_3 - \dot{y}_{in})c_f + (y_4 - y_{in})k_g + (\dot{y}_4 - \dot{y}_{in})c_g}{\ddot{y}_{in} \cdot \sum_i^{b, c, I, II, III, IV} m_i}, \quad (2)$$

where the numerator is the mathematical expression of the force at the driving-point, while the denominator is the imposed acceleration multiplied by the total mass of the model.

2.3. Optimization Procedure

The optimization procedure is based on minimizing the difference between experimental and simulated signals [8,29]. The initial guess values for the model elements were selected from previous studies: stiffness ($k_{b...g}$) and damping ($c_{b...g}$) were from Case β [12], while stiffness ($k_{a,h}$) and damping ($c_{a,h}$) were from model 2a [24]. The total parameter estimation of stiffness ($k_{a...h}$) and damping ($c_{a...h}$) was performed using a least-square algorithm (LSQ) applied to 13 subjects for natural COP position, 15 subjects for leaning forward COP position, and ten subjects for leaning backward COP position. The number of subjects for each COP position differs due to the availability of experimental data. In this study, only subjects with a full transmissibility dataset were included, and when a transmissibility measurement was not available, the respective subject was excluded from the optimization procedure.

The initial conditions of the model DOF were: $\theta_1 = 49^\circ$, $\theta_2 = 69^\circ$, $\theta_3 = 82^\circ$, $\theta_4 = 0^\circ$, $y_A = L_I \cos(\theta_1)$ m, $y_B = y_A + 0.05$ m and $y_C = y_B + 0.02$ m. The parameter limits were from 0.1 to 10 times the initial parameter values. The optimization procedure was repeated for each subject ten times, starting from random initial conditions. To define the LSQ objective function transmissibility and apparent mass errors computed as Equations (3) and (4):

$$\varepsilon_{AM} = \frac{1}{20} \sum_{f=2}^{20} \left| (AM_f - \widetilde{AM}_f)^2 \right|, \quad (3)$$

and

$$\varepsilon_T = \frac{1}{455} \sum_{f=10}^{100} \sum_{i=1}^5 \left| (T_f^i - \tilde{T}_f^i)^2 \right|, \quad (4)$$

where \widetilde{AM}_f and AM_f are respectively the simulated and measured [16] normalized apparent mass at frequency f . \tilde{T}_f^i and T_f^i are respectively the simulated and measured [15,17] foot transmissibility at location i and frequency f .

The LSQ objective function was defined as Equation (5):

$$F = \sqrt{w_{AM}\varepsilon_{AM} + w_T\varepsilon_T}, \quad (5)$$

where to apply the same weight to both apparent mass (w_{AM}) and transmissibility (w_T) in F , were selected as 26 and 1, respectively. These weighting factors were adjusted according to the experimental data collected. The optimized stiffness and damping values were used to compute the simulated transmissibility and apparent mass curves. The modulus reconstruction error for apparent mass was computed to evaluate the goodness of fit for the simulated curves, as Equation (6):

$$\epsilon_{AM}^m = \sqrt{\frac{1}{20} \sum_{f=2}^{20} \left(\left| \widetilde{AM}(f) \right| - |AM(f)| \right)^2}, \quad (6)$$

and reconstruction errors of the transmissibility modulus (m) for each position i were computed as Equation (7):

$$\epsilon_{T,i}^m = \sqrt{\frac{1}{91} \sum_{f=10}^{100} \left(\left| \widetilde{T}_i(f) \right| - |T_i(f)| \right)^2}. \quad (7)$$

At the end of the optimization loop, the subjects with reconstruction errors (ϵ) of the apparent mass modulus higher than 0.1 or the transmissibility modulus higher than 0.5 were excluded from the following analysis. It was observed that errors higher than 0.1 showed an underestimated simulated apparent mass magnitude around 5 Hz. A similar effect was observed for simulated transmissibility when the error was higher than 0.7. Thus, optimized subjects with ϵ_{AM}^m higher than 0.1 and $\epsilon_{T,i}^m$ higher than 0.7 were excluded from further analysis.

A first optimization of the FAS parameters underlined the variability of k_c and c_c , depending on the variability of experimental transmissibility measurements from the toes (Figure 3). To reduce the variability of the overall parameters, the parameters k_c and c_c were fixed to the median value computed in the first optimization as $130 \text{ N} \cdot \text{m}^{-1}$ and $740 \text{ N} \cdot \text{s} \cdot \text{m}^{-1}$ for natural, $65 \text{ N} \cdot \text{m}^{-1}$ and $2800 \text{ N} \cdot \text{s} \cdot \text{m}^{-1}$ for leaning forward, $40 \text{ N} \cdot \text{m}^{-1}$ and $43,000 \text{ N} \cdot \text{s} \cdot \text{m}^{-1}$ for leaning backward. Then, a second optimization found the 14 remaining parameters presented in Section 3. Both first and second optimization used the same initial conditions and guess values described above. The only difference between the two optimizations was that the second optimization was limited to 14 parameters. The variability of the optimized parameters between all subjects and COP positions has been visualized using boxplots for stiffness (k_e , k_f , k_g and k_d) and damping (c_e , c , c_g and c_d).

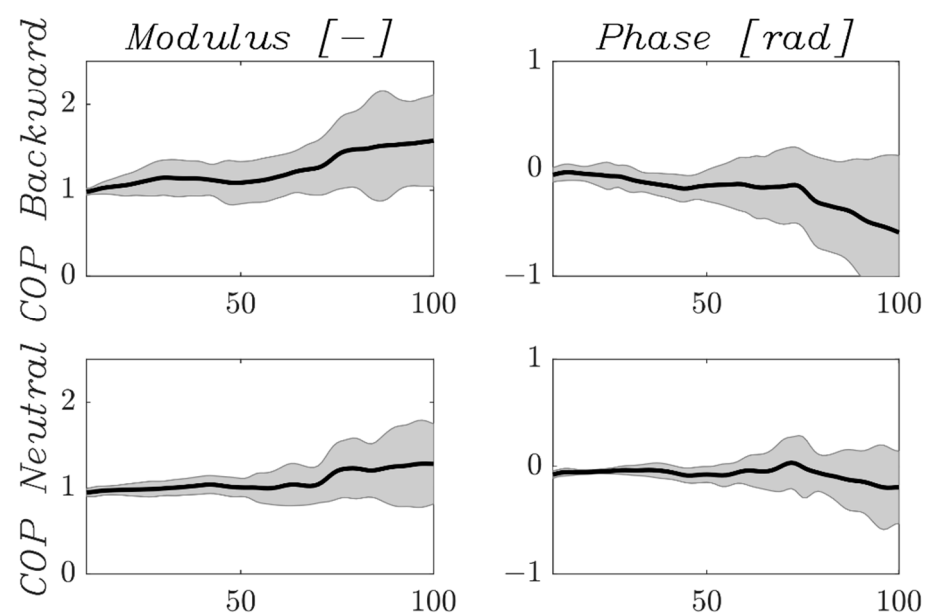


Figure 3. Cont.

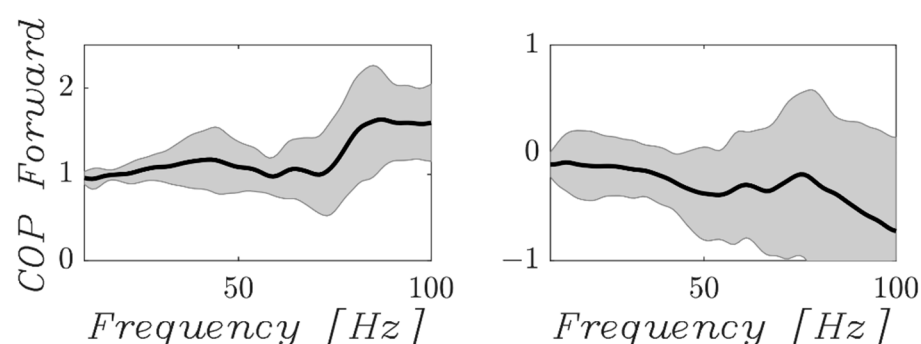


Figure 3. Measured amplitude and phase of the vibration transmissibility of the toes. Transmissibility is reported for all three COP positions (backward, natural and forward). The mean value (solid black line) and variability (grey cloud), representing a 95% confidence interval, were computed among the subjects included in the optimization procedure.

3. Results

Simulated curves and the respective reconstruction error have been computed for all subjects included in the optimization procedure. Curves for one subject with their COP in the natural standing position are illustrated in Figure 4. The reconstructed error of the modulus is highest for the forefoot ($\epsilon_{T,4}^m = 0.35$) and lowest for the normalized apparent mass ($\epsilon_{AM}^m = 0.038$) in this example.

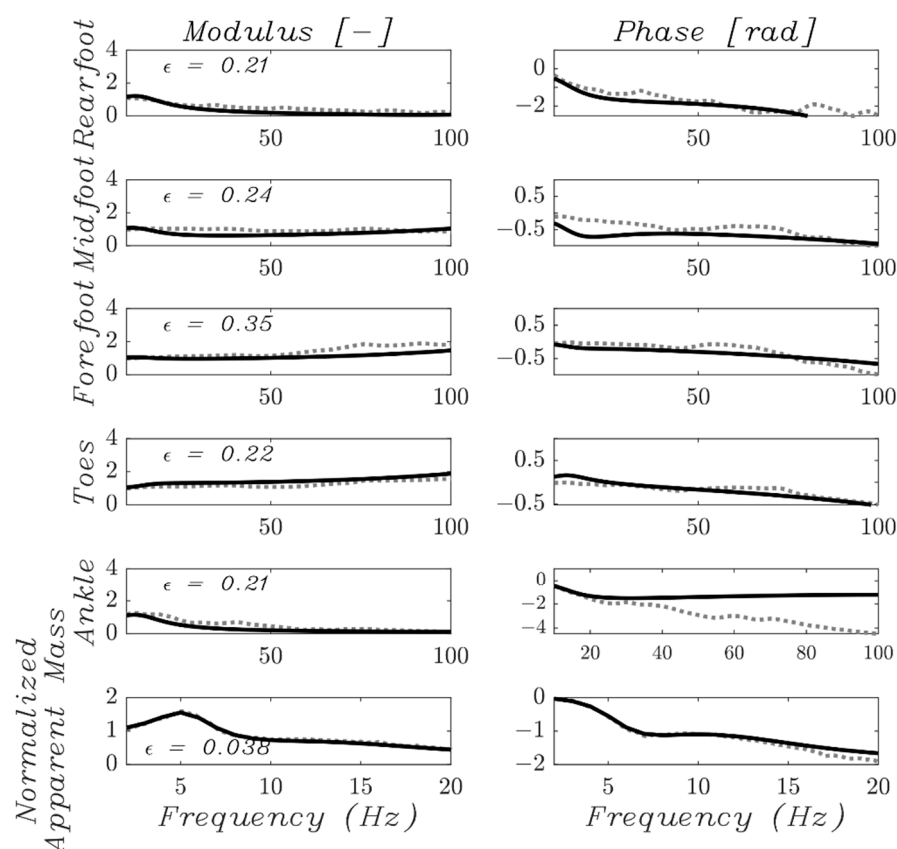


Figure 4. Simulated (black curves) and experimental (grey curves) amplitude and phase of five transmissibility and the apparent mass of one subject in natural standing posture. The reconstruction errors (ϵ_{AM}^m and $\epsilon_{T,i}^m$) are also reported for each amplitude.

Throughout the following description of the results, the superscripts 'F', 'N' and 'B' of the coefficient simulated values refer to leaning forward, natural and leaning backward

values, respectively (i.e., k_e^F refers to the stiffness of the heel fat pad in the leaning forward posture). The variability of each parameter is calculated among all included subjects. Rearfoot stiffness (k_e) variability is comparable for the three postures, and a decreasing trend is found passing from the backward leaning to the forward leaning posture (Figure 5: median values equal to $k_e^B = 3.5 \times 10^5 \text{ N}\cdot\text{m}^{-1}$, $k_e^N = 2.3 \times 10^5 \text{ N}\cdot\text{m}^{-1}$ and $k_e^F = 1.9 \times 10^5 \text{ N}\cdot\text{m}^{-1}$). An outlier is noticed in a natural posture with k_e^N close to $1.0 \times 10^6 \text{ N}\cdot\text{m}^{-1}$. An opposite trend is shown by forefoot stiffness (k_f) (Figure 5: median values equal to $k_f^B = 5.8 \times 10^5 \text{ N}\cdot\text{m}^{-1}$, $k_f^N = 8.5 \times 10^5 \text{ N}\cdot\text{m}^{-1}$ and $k_f^F = 1.0 \times 10^6 \text{ N}\cdot\text{m}^{-1}$). In this case, the parameter variability is comparable for natural and forward leaning postures, while backward leaning variability is larger. Toes stiffness (k_g) has a variability of several orders of magnitude in all postures with no trend (Figure 5: median values equal to $k_g^B = 8.1 \times 10^4 \text{ N}\cdot\text{m}^{-1}$, $k_g^N = 1.1 \times 10^5 \text{ N}\cdot\text{m}^{-1}$ and $k_g^F = 3.4 \times 10^4 \text{ N}\cdot\text{m}^{-1}$). The plantar aponeurosis stiffness (k_d) shows similar median values in all postures without any trend.

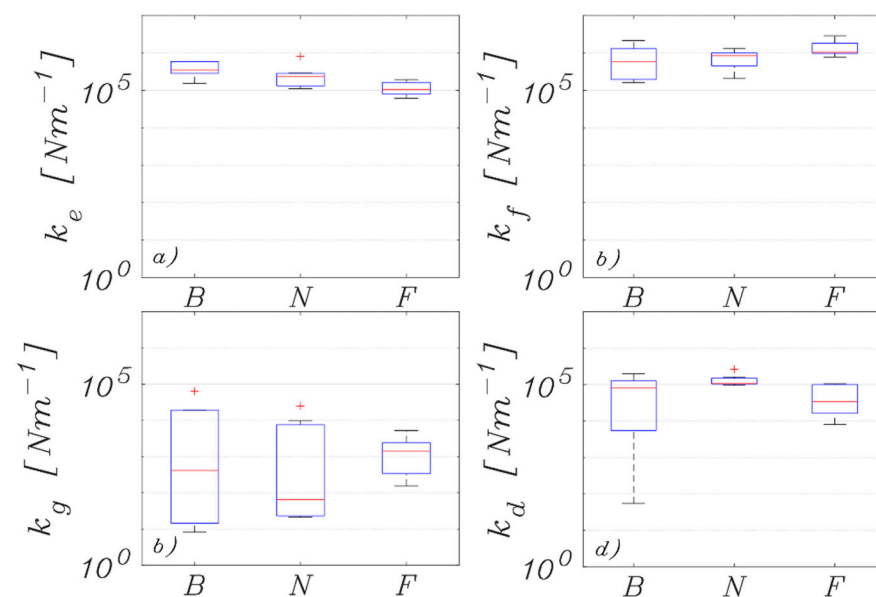


Figure 5. Box plot analysis of: (a) the stiffness for the rearfoot sole (k_e), (b) midfoot sole (k_f), (c) forefoot sole (k_g) and (d) the plantar aponeurosis (k_d) when the COP was in the backward (B), natural (N) and forward (F) positions.

Rearfoot damping (c_e) shows reduced variability for the COP in the forward and natural positions, while the backward COP position variability is between $0.02 \text{ N}\cdot\text{s}\cdot\text{m}^{-1}$ and $290 \text{ N}\cdot\text{s}\cdot\text{m}^{-1}$ (Figure 6). Similar behavior is observed for the sole of the midfoot damping (c_f), but a trend is not clear for either parameter. The toe damping (c_g) variability was found to vary with several orders of magnitude with median values $c_g^B = 2.5 \times 10^3 \text{ N}\cdot\text{s}\cdot\text{m}^{-1}$, $c_g^N = 2.7 \times 10^3 \text{ N}\cdot\text{s}\cdot\text{m}^{-1}$ and $c_g^F = 3.5 \times 10^3 \text{ N}\cdot\text{s}\cdot\text{m}^{-1}$ (Figure 6). Plantar aponeurosis damping (c_d) values and variability are comparable for all the postures, with median values of $c_d^B = 1.6 \times 10^3 \text{ N}\cdot\text{s}\cdot\text{m}^{-1}$, $c_d^N = 1.7 \times 10^3 \text{ N}\cdot\text{s}\cdot\text{m}^{-1}$ and $c_d^F = 1.9 \times 10^3 \text{ N}\cdot\text{s}\cdot\text{m}^{-1}$ (Figure 6).

The rotational stiffness (k_b) and damping (c_b) do not show a median value trend for the three COP positions (Table 2). Stiffness variability was of several orders of magnitude for all the postures while damping variability was reduced for natural and forward leaning postures. Stiffness between m_b and the ankle (k_a) resulted in high median values, which is close to the equivalent stiffness of bone, for all the three COP positions, with less than one order of magnitude variability. Damping between m_b and the ankle (c_a) values increased from the backward leaning to forward leaning COP positions. Stiffness between m_b and m_c (k_h) and damping (c_h) has shown small variability with all quartile values close to median values (Table 2).

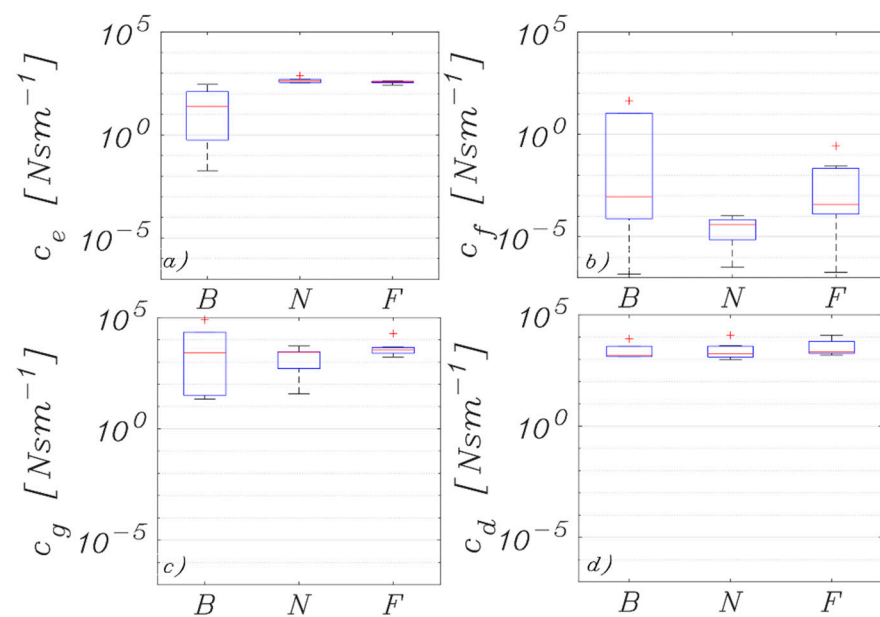


Figure 6. Box plot analysis of: (a) the damping for the rearfoot sole (c_e), (b) midfoot sole (c_f), (c) forefoot sole (c_g) and (d) the plantar aponeurosis (c_d) when the COP was in the backward (B), natural (N) and forward (F) positions.

Table 2. Median, 25th and 75th quartiles for the stiffness and damping at three locations (k_b , k_a , k_h , c_b , c_a and c_h) when the COP was in the backward (B), natural (N) and forward (F) positions.

Parameter [Unit]	Description	COP Position	Quartile 1	Median	Quartile 3
k_b [N·rad ⁻¹]	Stiffness of segments II/III joint	B	0.46	9.7×10^2	1.1×10^5
		N	0.20	0.45	7.1×10^3
		F	0.36	1.8	94
k_a [N·m ⁻¹]	Stiffness between m_b and ankle	B	2.1×10^5	3.3×10^5	5.5×10^6
		N	1.5×10^5	3.1×10^5	5.4×10^5
		F	1.4×10^6	3.2×10^6	3.7×10^7
k_h [N·m ⁻¹]	Stiffness between m_b and m_c	B	2.0×10^4	2.2×10^4	2.2×10^4
		N	2.0×10^4	2.1×10^4	2.1×10^4
		F	2.0×10^4	2.1×10^4	2.4×10^4
c_b [N·s·rad ⁻¹]	Damping of segments II/III joint	B	0.01	0.02	1.9×10^4
		N	0.01	0.05	0.12
		F	0.02	0.04	0.09
c_a [N·s·m ⁻¹]	Damping between m_b and ankle	B	4.0×10^3	1.5×10^4	3.4×10^5
		N	1.7×10^4	5.8×10^4	4.2×10^5
		F	1.1×10^5	8.0×10^5	2.8×10^6
c_h [N·s·m ⁻¹]	Damping between m_b and m_c	B	4.2×10^2	4.6×10^2	4.9×10^2
		N	3.8×10^2	4.0×10^2	4.4×10^2
		F	3.9×10^2	4.3×10^2	4.5×10^2

4. Discussion

A two-dimensional lumped-parameter model of a standing person and the FAS, which included four-foot segments [12], was optimized using reference functions from previously collected apparent mass [16] and transmissibility [15,17] to explore the effects of altering the COP location. The model parameters were optimized to fit apparent mass and five-foot transmissibility measurements of standing upright subjects with the COP in a forward ($n = 15$), natural ($n = 13$) and backward ($n = 10$) position. Optimizing a model of the FAS using altering COP locations will prove useful for further evaluating effective control strategies to isolate the foot from vibration exposure and hopefully avoid vibration-induced injury.

In general, modelling results showed that when the COP is moved forward towards the toes the stiffness values forefoot increased, conversely the stiffness of the rearfoot decreased. The opposite resulted when the COP was concentrated towards the rearfoot: the stiffness at the forefoot decreased, while the stiffness of rearfoot increased. This effect is reasonable, as the mass distribution on the foot regions changes accordingly to COP position [13]. For instance, in the forward COP position, the mass distribution is closer to the toes, causing a compression state in the musculature and ligaments of the superior portion of the forefoot (k_b and k_c). The compression state of the soft tissue can result from: (1) the muscular organization to maintain the standing posture where muscular activation results in muscle shortening and co-contraction of agonist and antagonist muscles; and/or (2) the change in the mass distribution with a more global view of the system conveying that the rest of the body will apply a compression force on the forefoot or the rearfoot. Additionally, the increase of stiffness values associated with higher contact force is in accordance the results given by a biodynamic model of the hand in case of grip only and grip with push conditions [30].

More specifically, there were three Kelvin–Voigt models associated with the soft tissue on the sole of the foot: at the rearfoot sole (i.e., heel or plantar) (k_e and c_e), the metatarsal/phalange joint (i.e., distal head of the metatarsals) (k_f and c_f) and the distal phalanges (i.e., tip of the toes) (k_g and c_g). As previously suggested and anticipated, the stiffness of the heel fat pad increased when the COP was backward and decreased as the COP moved forward towards the toes [13]. Stiffness of the rearfoot fat pad ($k_e^B = 3.5 \times 10^5 \text{ N}\cdot\text{m}^{-1}$, and $k_e^F = 1.9 \times 10^5 \text{ N}\cdot\text{m}^{-1}$) are in accordance with natural value $k_e^N = 2.3 \times 10^5 \text{ N}\cdot\text{m}^{-1}$, comparable with the value reported by [30]. The damping characteristics of the heel fat pad were more variable in the backward COP position than in the natural and forward COP positions. The heel fat pad is a specific tissue comprised of adipose chambers enclosed by fibrous septa to absorb impacts, as such the damping characteristics can change when pressure is applied to heel [31].

Stiffness of the soft tissue of the forefoot, at the distal head of the metatarsals (k_f) remained relatively the same regardless of the COP position, while the damping (c_f) varied between COP positions, with the greatest variability in the backward COP position. The stiffness at the tip of the toes (k_g) was lower than that at the distal head of the metatarsals regardless of the COP position. As the distal heads of the metatarsals are the weight bearing portion of the toes, this modelling result is in line with the anatomical differences at these two locations on the toes. The optimization of the contact stiffness of the toes (k_g) led to a higher parameter variability than at the distal head of the metatarsals (k_f) which could be due to the experimental variability of toes transmissibility [17]. In the optimization procedure, a reflection of this high variability effect on the equivalent rotational stiffness (k_b), that is linked to the toes DOF through k_c .

Forefoot sole stiffness has a higher value in leaning forward COP position with respect to rearfoot value ($k_f^F = 1.0 \times 10^6 \text{ N}\cdot\text{m}^{-1}$, $k_e^F = 1.9 \times 10^5 \text{ N}\cdot\text{m}^{-1}$). Damping values related to the soft tissues (c_e , c_f) are lower than the respective stiffness values, as evidenced by [32,33]. Whereas the contact damping of toes (c_g) is higher than the respective stiffness (k_g) because the toes are not gripping the vibrating surface and have little mass distribution to the tips

of the toes. Rearfoot stiffness (k_e) value in all COP positions was lower than the midfoot stiffness value (k_f), which is in accordance with the previously developed model [12].

Stiffness and damping between m_b and the ankle (k_a and c_a) and between m_c and m_b (k_h and c_h) values were comparable with the one proposed by [19] (Table 3). The main differences are linked to dynamical response of the upper body and had an effect in the reconstruction of the apparent mass curve. The maximum accepted reconstruction error equal to 0.1 underestimated the magnitude resonance value even of 15%.

Table 3. Comparison between upper body parameters optimized in this study and those of previously published work [19].

Parameter	Reference [19]	COP Position (Median)		
		Backward	Natural	Forward
k_a [$\text{N}\cdot\text{m}^{-1}$]	1.5×10^5	3.3×10^5	3.1×10^5	3.2×10^6
k_h [$\text{N}\cdot\text{m}^{-1}$]	1.9×10^4	2.2×10^4	2.1×10^4	2.1×10^4
c_a [$\text{N}\cdot\text{s}\cdot\text{m}^{-1}$]	1.3×10^3	1.5×10^4	5.8×10^4	8.0×10^4
c_h [$\text{N}\cdot\text{s}\cdot\text{m}^{-1}$]	4.1×10^2	4.6×10^2	4.0×10^2	4.3×10^2

Given the variability of the optimized parameters, the significant values of the Kelvin–Voigt models reported are an indication of real equivalent damping and stiffness of human ligaments and tissues. All model simulations are limited by their reference functions. In this case, the experimental transmissibility and apparent mass functions were from separate experiments with different exposure frequencies [15–17], which is mostly due to the limitations of force transducers for measuring apparent mass simultaneously during higher frequency vibration exposure. The transmissibility functions also had high inter-subject variability, which could have been due to the active contribution of muscles needed to stabilize the posture, or the difference in participant anthropometry [15,17]. With the advances made in reducing the number of anatomical locations required for capturing FTV exposure [23], future laboratory experiments could involve more conditions and a variety of populations.

This model sets the foundation of reported model parameters for a lumped-parameter model of the FAS to FTV exposure with varying COP locations. As this model also has the greatest variability in parameter values when the COP is backwards [13], the soft tissue at the heel (i.e., plantar fat pad) needs to be modelled differently in the future. There is also the potential that these tissues can be modelled more effectively with finite-element modelling like hand-transmitted vibration models [22]. Once this tissue has been effectively modelled boot, insole and mat material characteristics can be simulated and tested prior to creation and distribution. This proactive approach to designing engineering controls has been determined to be successful in mitigating occupational vibration exposure.

5. Conclusions

To explore the effects of altering the COP position on the biodynamic response of the foot when exposed to vibration while standing, a previously developed lumped-parameter model the FAS, which included four-foot segments [12], was optimized using reference functions from previously collected apparent mass [16] and transmissibility [15,17]. The model has reconstructed the apparent mass (frequency range: 2–20 Hz) and five-foot transmissibility measurements (frequency range: 10–100 Hz) with the COP in three different positions (backward, natural and forward). As anticipated, model element values differed based on the COP position. The most noteworthy differences occurred with the three Kelvin–Voigt elements used to represent the soft tissues of the foot sole: at the heel, metatarsal/phalange joint (i.e., distal head of the metatarsals), and distal phalanges (i.e., tip of the toes). Wherever the COP was concentrated (i.e., forward over the toes or backward over the heel), the stiffness increased. The stiffness decreased in the opposite elements when

the mass was not distributed over that anatomical area. These three stiffness values were estimated with similar inter-subject variability. The variability of the model parameters was always greatest when the COP was in the backward position or concentrated in the heel. This suggests future FAS models need to more clearly address how the soft tissue of the plantar fat pad is modelled. Model limitations could be due to the two-dimensional approximation: further studies could include three-dimensional modeling of the foot to better approximate the soft tissues of the heel, metatarsals and toes.

Author Contributions: Conceptualization: S.M. and M.T. Methodology: S.M. and D.C. Formal analysis: S.M. Data curation: S.M., D.C. and K.G. Writing—original draft preparation: S.M. and D.C. Writing—review and editing: S.M., D.C., D.S. and K.G. Visualization: T.E. Supervision and Project administration: M.T. All authors have read and agreed to the published version of the manuscript.

Funding: This research received no external funding.

Conflicts of Interest: The authors disclose professional relationships with companies or manufacturers who will benefit from the results of the present study. The results of the study are presented clearly, honestly and without fabrication, falsification or inappropriate data manipulation.

References

1. Eger, T.; Thompson, A.; Leduc, M.; Krajnak, K.; Goggins, K.; Godwin, A.; House, R. Vibration induced white-feet: Overview and field study of vibration exposure and reported symptoms in workers. *Work* **2014**, *47*, 101–110. [[CrossRef](#)] [[PubMed](#)]
2. Harazin, B.; Grzesik, J. The transmission of vertical whole-body vibration to the body segments of standing subjects. *J. Sound Vib.* **1998**, *215*, 775–787. [[CrossRef](#)]
3. Leduc, M.; Eger, T.; Godwin, A.; Dickey, J.P.; House, R. Examination of vibration characteristics, and reported musculoskeletal discomfort for workers exposed to vibration via the feet. *J. Low Freq. Noise Vib. Act. Control* **2011**, *30*, 197–206. [[CrossRef](#)]
4. House, R.; Jiang, D.; Thompson, A.; Eger, T.; Krajnak, K.; Sauve, J.; Schweigert, M. Vasospasm in the feet in workers assessed for HAVS. *Occup. Med.* **2011**, *61*, 115–120. [[CrossRef](#)] [[PubMed](#)]
5. Thompson, A.M.S.; House, R.; Krajnak, K.; Eger, T. Vibration-white foot: A case report. *Occup. Med.* **2010**, *60*, 572–574. [[CrossRef](#)]
6. Tarabini, M.; Eger, T.; Goggins, K.; Moorhead, A.P.; Goi, F. Effect of the shoe sold on the vibration transmitted from the supporting surface of the feet. *Vibration* **2021**, *4*, 743–758. [[CrossRef](#)]
7. Griffin, M.J. *Handbook of Human Vibration*, 1st ed.; Academic Press: London, UK, 1990; p. 998.
8. Dong, R.G.; Welcome, D.E.; McDowell, T.W.; Wu, J.Z. Theoretical foundation, methods, and criteria for calibrating human vibration models using frequency response functions. *J. Sound Vib.* **2015**, *356*, 195–216. [[CrossRef](#)]
9. Kim, W.; Voloshin, A.S. Role of plantar fascia in the load bearing capacity of the human foot. *J. Biomech.* **1995**, *28*, 1025–1033. [[CrossRef](#)]
10. Wee, H.B. The Dynamic Model of the Foot and Ankle System. Master's Thesis, Lehigh University, Bethlehem, PA, USA, 2012.
11. Simkin, A.; Leichter, I. Role of the calcaneal inclination in the energy storage capacity of the human foot—a biomechanical model. *Med. Biol. Eng. Comput.* **1990**, *28*, 149–152. [[CrossRef](#)] [[PubMed](#)]
12. Chadeaux, D.; Goggins, K.; Cazzaniga, C.; Marzaroli, P.; Marelli, S.; Katz, R.; Eger, T.; Tarabini, M. Development of a two-dimensional dynamic model of the foot-ankle system exposed to vibration. *J. Biomech.* **2019**, *99*, 109547. [[CrossRef](#)] [[PubMed](#)]
13. Goggins, K.A.; Chadeaux, D.; Tarabini, M.; Arsenaault, M.; Lievers, W.B.; Eger, T. Four degree-of-freedom lumped parameter model of the foot-ankle system exposed to vertical vibration from 10 to 60 Hz with varying centre of pressure conditions. *Ergonomics* **2021**, *64*, 1–16. [[CrossRef](#)]
14. Wee, H.; Voloshin, A. Transmission of vertical vibration to the human foot and ankle. *Ann. Biomed. Eng.* **2013**, *41*, 1172–1180. [[CrossRef](#)] [[PubMed](#)]
15. Goggins, K.A.; Tarabini, M.; Lievers, W.B.; Eger, T.R. Biomechanical response of the human foot when standing in a natural position while exposed to vertical vibration from 10–200 Hz. *Ergonomics* **2019**, *62*, 644–656. [[CrossRef](#)] [[PubMed](#)]
16. Tarabini, M.; Saggin, B.; Scaccabarozzi, D.; Gaviraghi, D.; Moschioni, G. Apparent mass distribution at the feet of standing subjects exposed to whole-body vibration. *Ergonomics* **2013**, *56*, 842–855. [[CrossRef](#)]
17. Goggins, K.A.; Tarabini, M.; Lievers, W.B.B.; Eger, T.R. Standing centre of pressure alters the vibration transmissibility response of the foot. *Ergonomics* **2019**, *62*, 1202–1213. [[CrossRef](#)] [[PubMed](#)]
18. Salathé, E.P.; Arangio, G.A.; Salathé, E.P. A biomechanical model of the foot. *J. Biomech.* **1986**, *19*, 989–1001. [[CrossRef](#)]
19. Matsumoto, Y.; Griffin, M.J. Mathematical models for the apparent masses of standing subjects exposed to vertical whole-body vibration. *J. Sound Vib.* **2003**, *260*, 431–451. [[CrossRef](#)]
20. Busca, G.; Cappellini, A.; Manzoni, S.; Tarabini, M.; Vanali, M. Quantification of changes in modal parameters due to the presence of passive people on a slender structure. *J. Sound Vib.* **2014**, *333*, 5641–5652. [[CrossRef](#)]
21. Dong, R.G.; McDowell, T.W.; Welcome, D.E.; Warren, C.; Wu, J.Z.; Rakheja, S. Analysis of anti-vibration gloves mechanism and evaluation methods. *J. Sound Vib.* **2009**, *321*, 435–453. [[CrossRef](#)]

22. Dong, R.G.; Wu, J.Z.; Xu, Z.S.; Welcome, D.E.; Krajnak, K. A review of hand-arm vibration studies conducted by US NIOSH since 2000. *Vibration* **2021**, *4*, 482–528. [[CrossRef](#)]
23. Goggins, K.A.; Oddson, B.E.; Lievers, W.B.; Eger, T.R. Anatomical locations for capturing magnitude differences in foot-transmitted vibration exposure, determined using multiple correspondence analysis. *Theor. Issues Ergon. Sci.* **2020**, *21*, 562–576. [[CrossRef](#)]
24. Matsumoto, Y.; Griffin, M.J. Dynamic response of the standing human body exposed to vertical vibration: Influence of posture and vibration magnitude. *J. Sound Vib.* **1998**, *212*, 85–107. [[CrossRef](#)]
25. Isman, R.E.; Inman, V.T. Anthropometric Studies of the Human Foot and Ankle. *Foot Ankle* **1969**, *11*, 97–129.
26. Lee, Y.-C.; Lin, G.; Wang, M.-J.J. Evaluating gender differences in foot dimensions. In Proceedings of the Ergonomics for All: Celebrating PPCOE's 20 Years of Excellence—Selected Papers of the Pan-Pacific Conference on Ergonomics, PPCOE, Kaohsiung, Taiwan, 7–10 November 2010; pp. 9–13.
27. Zatsiorsky, V. *Kinematics of Human Motion*; Human Kinetics Publishers: Champaign, IL, USA, 2002.
28. Tarabini, M.; Solbiati, S.; Moschioni, G.; Saggin, B.; Scaccabarozzi, D. Analysis of non-linear response of the human body to vertical whole-body vibration. *Ergonomics* **2014**, *57*, 1711–1723. [[CrossRef](#)] [[PubMed](#)]
29. Subashi, G.H.; Matsumoto, Y.; Griffin, M.J. Modelling resonances of the standing body exposed to vertical whole-body vibration: Effects of posture. *J. Sound Vib.* **2008**, *317*, 400–418. [[CrossRef](#)]
30. Dong, R.G.; Dong, J.H.; Wu, J.Z.; Rakheja, S. Modeling of biodynamic responses distributed at the fingers and the palm of the human hand–arm system. *J. Biomech.* **2007**, *40*, 2335–2340. [[CrossRef](#)] [[PubMed](#)]
31. Fontanella, C.G.; Nalesso, F.; Carniel, E.L.; Natali, A.N. Biomechanical behaviour of plantar fat pad in healthy and degenerative foot conditions. *Med. Biol. Eng. Comput.* **2016**, *54*, 653–661. [[CrossRef](#)] [[PubMed](#)]
32. Dong, R.G.; Schopper, A.W.; McDowell, T.W.; Welcome, D.E.; Wu, J.Z.; Smutz, W.P.; Warren, C.; Rakheja, S. Vibration energy absorption (VEA) in human fingers-hand-arm system. *Med. Eng. Phys.* **2004**, *26*, 483–492. [[CrossRef](#)] [[PubMed](#)]
33. Reynolds, D.D.; Falkenberg, R.J. Three-and four-degrees-of-freedom models of the vibration response of the human hand. In *Vibration Effects on the Hand and Arm in Industry*; Wiley: New York, NY, USA, 1982; pp. 117–132.